9742 *Inorg. Chem.* **2009**, *48*, 9742–9753
DOI: 10.1021/ic9008575

Inorganic Chemistry
Article

Electronic Properties of a Cytosine Decavanadate: Toward a Better Understanding of Chemical and Biological Properties of Decavanadates

Nada Bošnjaković-Pavlović,[†,‡] Anne Spasojević-de Biré,[*,†] Isabel Tomaz,[§] Nouzha Bouhmaida,[∥] Fernando Avecilla,[⊥] Ubavka B. Mioč,[‡] João Costa Pessoa,[§] and Nour Eddine Ghermani[*,†,¶]

[†]*Laboratoire Structures, Propriétés et Modélisation des Solides* (*SPMS*), *UMR CNRS 8580, Ecole Centrale Paris, Grande Voie des Vignes, 92295 Châtenay-Malabry, France,* [‡]*Faculty of Physical Chemistry, University of Belgrade, P.O. Box 47, 11158 Belgrade, PAC 105305, Serbia,* [§]*Centro de Quimica Estrutural, Instituto Superior Tecnico, TU Lisbon, Av. Rovisco Pais, 1049-001 Lisboa, Portugal,* [∥]*Laboratoire des Sciences des Matériaux* (*LSM*) *Université Cadi Ayyad, Faculté des Sciences Semlalia, Boulevard Prince Moulay Abdallah, BP 2390, 40000 Marrakech, Morocco,* [⊥]*Departamento de Química Fundamental, Facultad de Ciencias, Universidade da Coruña, Campus da Zapateira s/n, 15071 A Coruña, Spain, and* [¶]*Laboratoire de Physique Pharmaceutique, UMR CNRS 8612, Faculté de Pharmacie, 5 rue Jean-Baptiste Clément, 92296 Châtenay-Malabry, France*

Received May 4, 2009

We have synthesized and crystallized a cytosine-decavanadate compound, Na_3 $[V_{10}O_{28}]$ $(C_4N_3OH_5)_3(C_4N_3OH_6)_3 \cdot 10H_2O$, and its crystal structure has been determined from a single-crystal X-ray diffraction. A high resolution X-ray diffraction experiment at 210 K (in $P\bar{1}$ space group phase) was carried out. The data were refined using a pseudo-atom multipole model to get the electron density and the electrostatic properties of the decavanadate-cytosine complex. Static deformation density maps and Atoms in Molecules (AIM) topological analysis were used for this purpose. To get insight into the reactivity of the decavanadate anion, we have determined the atomic net charges and the molecular electrostatic potential. Special attention was paid to the hydrogen bonding occurring in the solid state between the decavanadate anion and its environment. The comparison of the experimental electronic characteristics of the decavanadate anions to those found in literature reveals that this anion is a rigid entity conserving its intrinsic properties. This is of particular importance for the future investigations of the biological activities of the decavanadate anion.

Introduction

Polyoxometalates (POMs) are a fascinating class of metal−oxygen cluster compounds with a unique structural variety and interesting properties, which are used in different fields. Among the different synthesized POMs, we have focused on the polyoxovanadates (POVs). The vanadium has been chosen for its relative low toxicity in biological media. Interaction analysis of vanadate and cellular proteins is difficult under physiological conditions because the aqueous vanadate species are pH, temperature, buffer, and vanadate concentration dependent.[1] In biological systems, vanadium(V) containing solutions exhibit different oligomeric vanadate species in equilibrium, for example, monomeric, dimeric, tetrameric, and decameric, each with different states of protonation and conformation, depending on experimental conditions. It is believed that almost 98% of vanadium in cells is present in the vanadium(IV) oxidation state, the intracellular concentration of vanadium(V) being very low for the formation of vanadate oligomers.[2] This is probably the reason why in vivo toxicological studies of vanadate oligomers are scarce. However, it is proposed that once formed, decavanadate (DV) eventually converts to the labile oxovanadates, but the rate can be very slow and effectively allows DV to exists for some time under physiological conditions.[3] Vanadium half-life in the intracellular medium has been estimated to be approximately half an hour,[4] enough to allow to study its effects not only in vitro, but also in vivo.[5,6] However its presence in significant amounts can be explained by the existence of special cell compartments where vanadium can be accumulated and preserved from

*To whom correspondence should be addressed. E-mail: anne.spasojevic@ecp.fr.

(1) Crans, D. C. *Comments Inorg. Chem.* **1994**, *16*, 1.
(2) Soares, S. S.; Martins, H.; Aureliano, M. *Arch. Environ. Contam. Toxicol.* **2006**, *50*, 60.
(3) Aureliano, M.; Crans, D. C. *J. Inorg. Biochem.* **2009**, *103*, 536.
(4) Chasteen, N. D.; Grady, J. K.; Hoolway, C. E. *Inorg. Chem.* **1986**, *25*, 2754.
(5) Soares, S. S.; Aureliano, M.; Joaquim, N.; Coucelo, J. M. *J. Inorg. Biochem.* **2003**, *94*, 285.
(6) Aureliano, M.; Joaquim, N.; Sousa, A.; Martins, H.; Coucelo, J. *J. Inorg. Biochem.* **2002**, *90*, 159.

 Published on Web 09/18/2009

decomposition (protective "cage"). This can be explained by hydrogen-bonding interactions with surrounding molecules, like proteins or macrocyclic ligands.[7]

Several studies report that DV has a strong inhibitory effect on several enzymes, when compared to other oligomers:[8−10] inhibition of Ca^{2+}ATPase,[11−14] Na,K-ATPase,[15] muts ATPase,[16] myosin ATPase,[17−21] acid phosphatase A,[22] and other biological targets.[23−29] It has also been recently reported that DV can act as an insulin mimetic agent.[30,31] Aureliano et al. have formulated the hypothesis that mytochondria might be a target for DV species.[32] A complete review of biological activities of DV is given in a recent review of Aureliano et al.[3]

Investigations of POVs in the presence of enzymes and proteins can provide additional information on their mode of action. Many studies illustrate the importance of the noncovalent interactions between DV and peptides.[33−36] DV interacts very strongly with positively charged proteins. Therefore, the study of POV containing organic molecules is important, particulary the role of the organic cations in the structure of the DV, and understanding the direct interactions of vanadate with cellular proteins and enzymes may be an important key to reveal the physiological functions of vanadium oxoanions. Since the biological properties also result from interactions with viral enzymes or with viral cell envelopes, the understanding of these interactions at a molecular level is essential for the interpretation and the development of potent compounds with selective enzymatic affinity.

It has been demonstrated that accurate electron density can give pertinent informations on the interactions between potent drug and their biological targets.[37−42] Experimental X-ray determination of the accurate electron density in compounds containing transition metals has grown as a major area in the past few years. Most of the progress is due to the recent availability of fast devices like area detectors which provide full and very accurate data sets in short times even for crystals with large unit-cells. The fact that deformation density studies require optimal diffraction data quality and that 3d transition metals present special problems when refining the deformation density, because of the significantly different radial extension of the 3d and 4s valence orbitals, could explain that there are very few papers dealing with experimental deformation density of vanadate compounds.[43−45]

Besides experimental studies, theoretical calculations have already been performed for an isolated $[V_{10}O_{28}]^{6-}$ anion.[46−49] As this anion may possess different protonation sites, spectroscopic and structural studies were performed to localize the protonation sites of the DVs.[50,51] The goal of these calculations is to investigate the electronic structure of the POV anion and to get a quantitative determination of the reactivity of the six external sites of the oxygen atoms. It was found that the double-linked and triple-linked oxygen atoms are those which are most susceptible of protonation owing to the basicity of these atoms compared with that of the terminal atoms. The topography of the electrostatic potential (EP) distribution in the accessible region of the molecules is expected to provide informations on the approach of reagents, either electrophilic, dipolar, or nucleophilic.

We have already studied the crystal structure and the electrostatic properties of the $(NH_4)_6[V_{10}O_{28}]\cdot 6H_2O$ derived

(7) Farahbakhsh, M.; Schmidt, H.; Rehder, D. *Chem. Ber.* **1997**, *130*, 1123.
(8) Ramos, S.; Manuel, M.; Tiago, T.; Gandara, R. M. C.; Duarte, R.; Moura, J. J. G.; Gutiérrez-Merino, C.; Aureliano, M. *J. Inorg. Biochem.* **2006**, *100*, 1734.
(9) Fraqueza, G.; Rito, E.; Brissos, R.; Tiago, T.; Martins, J.; Duarte, R. O.; Moura, J. J.; Aureliano, M. *6th Int. Vanadium Symp.* **2008**, 46.
(10) Brissos, R.; Fontes, F. L.; Martins, H.; Fraqueza, G.; Tiago, T.; Martins, J.; Duarte, R. O.; Moura, J. G.; Aureliano, M. *6th Int. Vanadium Symp.* **2008**, P44.
(11) Csermely, P.; Varga, S.; Martonosi, A. *Eur. J. Biochem.* **1985**, *150*, 455.
(12) Csermely, P.; Martonosi, A.; Levy, G. C.; Ejchart, A. J. *Biochem. J.* **1985**, *230*, 807.
(13) Aureliano, M. *J. Inorg. Biochem.* **2000**, *80*, 145.
(14) Krstić, D.; Čolović, M.; Bosnjaković-Pavlović, N.; Spasojević-de Biré, A.; Vasić, V. *Gen. Physiol. Biophys.*, **2009**, in press.
(15) Rice, W. J.; Young, H. S.; Martin, D. W.; Sachs, J. R.; Stokes, D. L. *Biophys. J.* **2001**, *80*, 2187.
(16) Pezza, R. J.; Villarreal, M. A.; Montich, G. G.; Argarana, C. A. *Nucleic Acids Res.* **2002**, 4700.
(17) Aureliano, M. *J. Inorg. Biochem.* **2000**, *80*, 141.
(18) Tiago, T.; Aureliano, M.; Duarte, R. O.; Moura, J. J. G. *Inorg. Chim. Acta* **2002**, 339.
(19) Tiago, T.; Aureliano, M.; Guttierrez-Merino, C. G. *Biochemistry* **2004**, *43*, 5551.
(20) Tiago, T.; Aureliano, M.; Moura, J. J. *J. Inorg. Biochem.* **2004**, *98*, 1902.
(21) Tiago, T.; Martel, P.; Guttierrez-Merino, C. G.; Aureliano, M. *Bioch. Bioph. Acta* **2007**, *1774*, 474.
(22) Felts, R. L.; Reilly, T. J.; Tanner, J. J. *J. Biol. Chem.* **2006**, *281*, 30289.
(23) Boyd, D. W.; Kustin, K.; Niwai, M. *Biochim. Biophys. Acta* **1985**, *827*, 472.
(24) Pluskey, S.; Mahroof-Tahir, M.; Crans, D. C.; Lawrance, D. S. *Biochem. J.* **1997**, *321*, 333.
(25) Okamura, N.; Sakai, T.; Nishimura, Y.; Araki, S.; Yamaguchi, M.; Ishibashi, S. *Biol. Pharm. Bull.* **1999**, *22*, 799.
(26) Crans, D. C.; Sudkahar, K.; Zamborelli, T. J. *Biochemistry* **1992**, 6812.
(27) Messmore, J. M.; Raines, R. T. *Arch. Biochem. Biophys* **2000**, *381*, 25.
(28) Hir, M. *Biochem. J.* **1991**, *273*, 795.
(29) Soman, G.; Chang, Y. C.; Graves, D. J. *Biochemistry* **1983**, *22*, 4994.
(30) Garcia-Vicente, S.; et al. *Diabetes* **2007**, *57*, 486.
(31) Yraola, F.; Garcia-Vicente, S.; Marti, L.; Albericio, F.; Zorzano, A.; Royo, M. *Chem. Biol. Drug Des.* **2007**, *69*, 423.
(32) Aureliano, M.; Gandara, R. M. C. *J. Inorg. Biochem.* **2005**, *99*, 979.
(33) Meicheng, S.; Lifeng, W.; Youqi, T. *Sci. Sin., Ser. B* **1984**, *2*, 137.
(34) Crans, D. C. *Comments Inorg. Chem* **1994**, *16*, 35.
(35) Crans, D. C.; Mahroof-Tahir, M.; Anderson, O. P.; Miller, M. M. *Inorg. Chem.* **1994**, *33*, 5586.
(36) Wang, X.; Liu, H.-X.; You, X. X.; You, X.-Z. *Polyhedron* **1993**, *12*, 77.
(37) Spasojević-de Biré, A.; Kremenović, A.; Morgan, G.; Ghermani, N. E. *J. Phys. Chem.* **2002**, *A106*, 12170.
(38) Bouhmaida, N.; Dutheil, M.; Ghermani, N. E.; Becker, P. *J. Chem. Phys.* **2002**, *116*, 14.
(39) Ghermani, N. E.; Spasojević-de Biré, A.; Bouhmaida, N.; Ouharzoune, S.; Bouligand, J.; Layre, A.; Gref, R.; Couvreur, P. *Pharm. Res.* **2004**, *21*, 598.
(40) Overgard, J.; Hibbs, D. E. *Acta Crystallogr.* **2004**, *A60*, 480.
(41) Pizzonero, M.; Keller, L.; Dumas, F.; Ourevitch, M.; Morgan, G.; Ghermani, N. E.; Spasojević-de Biré, A.; Bogdanović, G. A.; d'Angelo, J. *J. Org. Chem.* **2004**, *69*, 4336.
(42) Firley, D.; Courcot, B.; Gillet, J. M.; Fraisse, B.; Zouhiri, F.; Desmaele, D.; D'Angelo, J.; Ghermani, N. E. *J. Phys. Chem.* **2006**, *B110*, 537.
(43) Bergstrom, O.; Gustafsson, T.; Thomas, J. O. *Solid State Ionics* **1998**, *110*, 179.
(44) Claiser, N. *DEA report*; Université Henri Poincaré: Nancy, France, 2000.
(45) Ozerov, R. P.; Streltsov, V. A.; Sobolev, A. N.; Figgis, B. N.; Volkov, V. L. *Acta Crystallogr.* **2001**, *B57*, 244.
(46) Rohmer, M. M.; Ernenwein, R.; Ulmschneider, M.; Wiest, R.; Benard, M. *Int. J. Quantum Chem.* **1991**, *40*, 723.
(47) Kempf, J. Y.; Rohmer, M. M.; Poblet, J. M.; Bo, C.; Benard, M. *J. Am. Chem. Soc.* **1992**, *114*, 1136.
(48) Rohmer, M. M.; Benard, M.; Blaudeau, J. P.; Maestre, J. M.; Poblet, J. M. *Coord. Chem. Rev.* **1998**, *178−180*, 1019.
(49) Henry, M. *J. Cluster Sci.* **2002**, *13*, 437.
(50) Brown, I. D.; Shannon, R. D. *Acta Crystallogr.* **1973**, *A29*, 266.
(51) Klemperer, W. G.; Shum, W. *J. Am. Chem. Soc.* **1977**, *99*, 3544.

from a κ-refinement.[52] In the present study, we report the crystal structure and electrostatic properties of Na_3 $[V_{10}O_{28}]$ $(C_4N_3OH_5)_3$ $(C_4N_3OH_6)_3 \cdot 10H_2O$ to have experimental evidence of the electrostatic properties derived from a co-crystal containing DV and an organic moiety (cytosine), and to relate the properties derived from a charge density study to the DV biological properties observed elsewhere.

Methodology

The crystal electron density is described as a superposition of aspherical pseudo-atoms according to the Hansen-Coppens formalism.[53,54] A κ-refinement[55] has been performed: P_{val} and κ parameters for the non-hydrogen atoms have been refined. Atomic net charges are derived from the experimental monopole population (P_{val}) after a κ-refinement and referenced as to the κ charges. A quantitative investigation of the bonding can be performed by means of a topological analysis according to the Atoms in Molecules (AIM) theory.[56] Following Bader[56] and Cremer et al.[57,58] the atomic interaction may be characterized through the values of density $\rho(r_{cp})$, the Laplacian $\nabla^2\rho(r_{cp})$, the kinetic energy density $G(r_{cp})$ and the local energy density $E(r_{cp})$ at the (3,-1) bond critical points (BCPs). The total energy density $H(r_{cp})$ is defined as the sum of a kinetic energy density $G(r_{cp})$ and a potential energy density $V(r_{cp})$. Abramov[59] has proposed the empirical formula $G(r_{cp}) = \frac{3}{10}(3\pi^2)^{2/3}\rho^{5/3}(r_{cp}) + \frac{1}{6}\nabla^2\rho(r_{cp})$ The Laplacian and the energy density are related by $2G(r_{cp}) + V(r_{cp}) = \frac{1}{4}\nabla^2\rho(r_{cp})$. The topological analysis of the electron density has been carried out using the NEWPROP program.[60,61] Experimental atomic net charges are derived from results of the topology of the charge density and referenced as to the AIM charges.[56] Further quantitative information on the electronic structures of metal atoms is obtained by d-orbital population analysis. Since the multipole terms in the Hansen-Coppens model[53] give an analytical description of the asphericity of the atomic charge density distribution, the d-orbital populations can be calculated directly from the multipole coefficients, P_{lm} according to the linear combination reported by Holladay et al.[62] The EP $\Phi(r)$ is computed using ELECTROS program[63] as the sum of the contributions of the positive nuclear charge Z_{at} located at R_{at} and the atomic electron density $\rho_{at}\Phi(r) = \sum_{atom}^{molecule} \frac{Z_{at}}{|r - R_{at}|} - \int \frac{\rho_{at}(r')}{|r - R_{at} - r'|} \, d^3r'$

Experimental Section

Synthesis. Heteropoly- and isopoly- anions have been prepared and isolated from both aqueous and non-aqueous solutions.[64] The most common preparative method involves acidification of aqueous solutions of simply oxoanion and the necessary heteroatoms; in many cases, it is necessary to control temperature or pH. Isolation of the polyanion from solution is generally achieved by addition of an appropriate counterion, commonly an alkali metal, ammonium, or tetraalkyl-ammonium.[65]

Cytosine (0.444 g, 4.00 mmol) was dissolved in about 40 mL of water at 50 °C. Sodium acetate trihydrate (0.964 g, 7.09 mmol) were added. The pH was in the range 5.5 to 5.8. A solution of salicylaldehyde (0.84 mL, 8 mmol) in 10 mL of ethanol was added dropwise and slowly, and the mixture was allowed to react for 1 h at 323 K.

A concentrated blue solution of oxidovanadium(IV) sulfate pentahydrate (0.862 g, 3.4 mmol) in 2.5 mL of water was then added dropwise. The reaction mixture became dark brown, and within a few minutes a heavy precipitation of a light green solid occurred, which was filtrated from the reaction mixture. This solid was most probably a mixture of the oxidovanadium(IV) bis-complex with salicylaldehyde ($V^{IV}O(Sal)_2$) and the oxidovanadium(IV) Schiff-base complex of salicylaldehyde and cytosine: $[V^{IV}O(Sal\text{-}Cyt)X]$; the identity/amount of anion X was not determined.

The filtrate was kept in a closed vessel at 279 K. A few weeks later reddish crystals suitable for X-ray diffraction analysis were separated from the liquid.

Data Collection, Data Reduction and Refinements. Crystallographic measurements were carried out at 210 K on a Siemens SMART CCD 1K diffractometer using Mo Kα radiation. This temperature was chosen because we have observed a phase transition occurring below 200 K from the $P\bar{1}$ (centrosymmetric) to the $P1$ space group (non-centrosymmetric). Resolution of the structure at 100 K does not allow us to get good quality results (localization of the all hydrogen atoms) because, in the $P1$ space group, the number of parameters is too high. A total of 38 400 frames were recorded with five different exposure time per frame (2, 5, 10, 20, 30 s) depending on the 2θ detector position; 221 309 reflections were collected. The absorption correction was applied using SADABS.[66] Data were sorted and merged using SORTAV,[67] giving 28 757 independent data up to a resolution of $[\sin\theta/\lambda]_{max} = 1.11$ Å^{-1} ($\theta_{max} = 75°$). The structure was solved by SIR92.[68] Na_3 $[V_{10}O_{28}]$ $(C_4N_3OH_5)_3$ $(C_4N_3OH_6)_3 \cdot 10H_2O$ crystallizes in the centro-symmetric space group $P\bar{1}$ at temperature > 210 K. All structural calculations were performed by using the SHELXL-97[69] program of the WINGX software package.[70] All atoms, except the hydrogen ones, were refined by using anisotropic thermal parameters. Thermal ellipsoid plots were obtained using the program ORTEP3.[71] The Hansen-Coppens multipole formalism,[53] implemented in the MOLLY program, was used for multipole and κ refinements.[55,72] Table 1 gives the experimental details of the single crystal experiment.

The radial terms used for V atoms were simple Slater functions, $R_{nl}(r) = Nr^{nl}\exp(-\xi_l r)$, $n = 4$ and $\xi = 5.99$ bohr^{-1} (for $l = 1$ to 4). The multipole terms up to hexadecapole were

(52) Bogdanović, G. A.; Bošnjaković-Pavlović, N.; Spasojević-de Biré, A.; Ghermani, N. E.; Mioč, U. *J. Serb. Chem. Soc.* **2007**, *72*, 545.
(53) Hansen, N.; Coppens, P. *Acta Crystallogr.* **1978**, *A34*, 909.
(54) Coppens, P. In *X-ray charge densities and chemical bonding*; International Union of Crystallography/Oxford University Press: Oxford, 1997.
(55) Coppens, P.; Guru Row, T. N.; Leung, P.; Stevens, E. D.; Becker, P; Yang, Y. W. *Acta Crystallogr.* **1979**, *A35*, 63.
(56) Bader, R. F. In *Atoms in molecules: A Quantum Theory*, Int. Series of Monographs in Chemistry 22; Oxford University Press: Oxford, 1990.
(57) Cremer, D.; Kraka, E. *Angew. Chem., Int. Ed. Engl.* **1984**, *23*, 627.
(58) Cremer, D.; Kraka, E. *Croat. Chem. Acta* **1984**, *57*, 1259.
(59) Abramov, Y. A. *Acta Crystallogr.* **1997**, *A53*, 264.
(60) Souhassou, M.; Blessing, B. *J. Appl. Crystallogr.* **1999**, *32*, 210.
(61) Souhassou, M. *Acta Crystallogr.* **2000**, *A56 (Supplement)*, s195.
(62) Holladay, A.; Leung, P.; Coppens, P. *Acta Crystallogr.* **1983**, *A39*, 377.
(63) Ghermani, N. E.; Bouhmaida, N.; Lecomte, C. *Internal report UMR CNRS 7036, Université Henri Poincaré, Nancy1, France and UMR CNRS 8612*; Université Paris XI: France, 1992−2001.
(64) Drechsel, E. *Ber.* **1887**, *20*, 1452.
(65) Chinea, E.; Dakternieks, D.; Duthie, A.; Ghilardi, C. A.; Gili, P.; Mederos, A.; Midollini, S.; Orlandini, A. *Inorg. Chim. Acta* **2000**, *298*, 172.
(66) *Bruker-AXS*; Analytical X-ray Instruments Inc.: Madison, WI, 1998.
(67) Blessing, R. H. *J. Appl. Crystallogr.* **1997**, *30*, 421.
(68) Altomare, A.; Cascarano, G.; Giacovazzo, C.; Guagliardi, A.; Burla, M. C.; Polidori, G.; Camalli, M. *J. Appl. Crystallogr.* **1994**, *27*, 435.
(69) Sheldrick, G. M. *SHELXL-97*; University of Göttingen: Göttingen, Germany, 1997.
(70) Farrugia, L. J. *Appl. Crystallogr.* **1999**, *32*, 837.
(71) Burnett, M. N.; Johnson, C. K. *ORTEP3*; Oak Ridge National Laboratory: Oak Ridge, TN, 1996.
(72) Coppens, P. *Coord. Chem. Rev.* **1985**, *65*, 285.

Table 1. X-ray Diffraction Experiment and Refinement Details[a]

chemical formula	$Na_3[V_{10}O_{28}](C_4N_3OH_5)_3(C_4N_3OH_6)_3 \cdot 10H_2O$
temperature (K)	210(1)
wavelength (Å)	0.71073
cell setting, space group	triclinic, $P\bar{1}$
Z	1
crystal size: (mm) × (mm) × (mm)	0.36 × 0.29 × 0.18
density (calculated) (Mg/m^3)	2.12
a (Å)	9.8526(1)
b (Å)	12.2227(1)
c (Å)	13.0852(1)
α (deg)	85.995(1)
β (deg)	80.110(1)
γ (deg)	70.954(1)
volume ($Å^3$)	1467.25(3)
$[\sin\theta/\lambda]_{max}$ ($Å^{-1}$)	1.11
scan width (deg)/scan method	0.15° / $\Delta\omega$ scan
crystal-to-detector distance (cm)	4.075
total frames/time per frame (s)	38400 /2 to 30
absorption correction	SADABS
total measured reflexions	221 309
R_{int} (F^2) before SADABS	0.071
R_{int} (F^2) after SADABS	0.031
number of reflexions used after SADABS	207 128
R_{int}	0.0276
no. of reflexions used in SHELX: all data/unique ($F_o > 4\sigma F_o$)	28 757/20 587
Spherical refinement: R(%)/R_w(%)/GOF/parameters	2.88/3.27/1.28/28
no. of reflexions used in MOLLY($I > 3\sigma(I)$)	18 394
κ refinement: R(%)/R_w (%)/GOF/parameters	2.76/2.97/1.16/20
Multipole refinement: R(%)/R_w (%)/GOF/parameters	2.32/2.34/0.91/505

[a] The value R_{int}, GOF, R and Rw are defined as $R_{int} = \sum_H[N_H/(N_H - 1)]^{1/2}\sum_{i=1}^{N_H}|I_i(H) - I_i^{mean}(H)|/\sum_{i=1}^{N_H}|I_i(H)|$. $I(H)$ is the observed reflection intensity for H vector. $N(H)$ is the number of equivalent and redundant reflections. $R = \sum||F_{obs}| - |F_{calc}||/\sum|F_{obs}|$, $R_w = [\sum w(F_{obs} - F_{calc})^2/\sum wF_{obs}^2]^{1/2}$, $GOF = \{\sum[w(F_{obs}^2 - F_{calc}^2)^2]/(m_{obs} - n_p)\}^{1/2}$. The statistical weight is $w = 1/\sigma^2(F_{obs})$ or $1/\sigma^2(F_{obs}^2)$ where σ^2 is the variance, m_{obs} and n_p are the number of observations and refined parameters, respectively.

included for the vanadium, up to octapole for nitrogen, carbon, and oxygen, and up to dipole for hydrogen atom. The local atomic frames for multipoles are given in the Supporting Information. The atomic core and valence scattering factors were taken from International Tables for X-ray Crystallography.[73] The core electron configuration was assumed to be He core for O, N, and C and Ar core for V.

It is well established[72,74−76] that 3d transition metals imply some difficulties when refining the deformation density because of the significantly different radial extension of the 3d and 4s valence orbitals. In view of these problems, it is a common practice to treat the 4s density as "core" density.[77] Therefore, we have tried different models. Models based on the $4s^23d^3$ electron configuration were initially examined, but gave chemically unrealistic populations; those based on the $4s^03d^5$ configuration gave significantly higher residuals in the density maps. The final model used was based on the $4s^03d^3$ configuration, where V^{2+} possesses 18 core electrons. To conserve the electron-neutrality, we have attributed the formal charges as follows: $[Na_3]^{3+}$ $[V_{10}O_{28}]^{6-}$ $[(C_4N_3OH_5)_3]^0$ $[(C_4N_3OH_6)_3]^{3+} \cdot 10H_2O$. In this approach, we have not authorized a charge transfer between the different ions of the compound. To minimize the number of refined parameters, we have imposed chemical constraints on water molecules: same populations and κ's for O and H, respectively. Reliability refinement factors are given in Table 1.

Results and Discussion

Selected interatomic distances of covalent and non-covalent interactions and topological analysis features are given in Tables 2 and 3; d orbital populations are reported in Table 4. Net atomic charges and EPs are given in Tables 5 and 6. Figure 1 gives the Oak Ridge Thermal Ellipsoid Plot (ORTEP) view of the crystal structure and labeling of the different atoms in the crystal structure. After the multipole refinement, the residual deformation electron density maps of the title compound are presented in Figure 2. The absence of significant peaks and holes of residual density indicates that the multipole model refinement is satisfactory. The maximum random errors according to Rees' formulism[78] is 0.0675 e $Å^{-3}$. The same trend is observed for the cytosine molecules, which, however, exhibit a significant accumulation of charge density around the N1c, C6c, and C2c. This poor quality is due to a local disorder leading to high values of thermal parameters which have been observed for these atoms.

Crystal Structure. The X-ray structural analysis reveals that the asymmetric unit of the title compound is composed of one-half of a DV anion, three molecules of cytosine, one and half of sodium, and five water molecules. Figure 1 depicts an ORTEP view of the crystal structure. DV is not protonated in the title compound, while in other crystal structures they could be protonated according to the formula $[V_{10}O_{28}H_x]^{(6-)-x}$ where $x = 1-5$.[79]

To compare the interatomic distances of the title compound with those in the literature, we have examined organic /organometallic Cambridge Structural Database (CSD)[80] with 37 data for 33 $[V_{10}O_{28}]^{6-}$ structures with agreement factor R less than 10%.[81] A search in the Inorganic Crystal Structure Database (ICSD)[82] has given 44 $[V_{10}O_{28}]^{6-}$ structures with agreement factor R less than 10%.[83] Interatomic bond distances and angles observed for the $[V_{10}O_{28}]^{6-}$ unit of the title compound exhibit a geometry which is quite similar to those found in previously reported structures of DV salts or co-crystals (Table 2). Therefore, one can consider that DV is a very rigid entity for which the interatomic distances are almost independent of the non-covalent interactions.

The asymmetric unit of the title compound contains three different molecules of cytosine (Figure 1a). The cytosine C is not protonated and is neutral. The cytosinium B

(73) *International Tables for X-ray Crystallography*; Kynoch Press: Birmingham, U.K. 1974, Vol. *IV*, p 103.
(74) Macchi, P.; Garlaschelli, L.; Martinengo, S.; Sironi, A. *J. Am. Chem. Soc*. **1999**, *121*, 10428.
(75) Ozerov, R. P.; Streltsov, V. A.; Sobolev, A. N.; Figgis, B. N.; Volkov, V. L. *Acta Crystallogr*. **2001**, *B57*, 244.
(76) Farrugia, L. J.; Mallinson, P. R.; Stewart, B. *Acta Crystallogr*. **2003**, *B59*, 234.
(77) Martin, M.; Rees, B.; Mitschler, A. *Acta Crystallogr*. **1982**, *B38*, 6.
(78) Rees, B. *Acta Crystallogr*. **1976**, *A32*, 483.
(79) See crystal structure studies references in Supporting Information, Table S2.
(80) Allen, F. H. *Acta Crystallogr*. **2002**, *B58*, 380.
(81) See crystal structure studies references in Supporting Information, Table S3.
(82) *ICSD*; Fachinformationszentrum (FIZ) Karlsruhe: Germany, 2007.
(83) See crystal structure studies references in Supporting Information, Table S4.

Table 2. Intramolecular Distances and Topology Analysis of the DV Anion[b]

			distance		ρ_{cp}		$\nabla^2\rho(r_{cp})$						
vanadium atoms	type of vanadium bonds	bond	this work	Kempf[47]	this work	Kempf[47]	this work	Kempf[47]	ε	λ_1	λ_2	λ_3	$H(r_{cp})$
V−Oa	VI−Oa *2.113*	V4−O61	2.0781(5)	2.116	0.52	0.47	8.87	7.59	0.01	−2.09	−2.08	13.04	−5.71
		V4−O61	2.1583(5)		0.44		6.90		0.05	−1.63	−1.56	10.09	−3.84
	VII−Oa *2.323*	V3−O61	2.3324(5)	2.316	0.32	0.28	4.36	5.52	0.03	−0.94	−0.91	6.2	−1.98
		V5−O61	2.2937(5)		0.34		4.72		0.10	−1.02	−0.93	6.68	−2.22
	VIII−Oa *2.244*	V1−O61	2.2679(6)	2.243	0.37	0.34	5.17	6.49	0.013	−1.19	−1.18	7.54	−1.94
		V2−O61	2.2414(5)		0.37		5.34		0.06	−1.13	−1.06	7.52	−2.40
V−Ob	VI−Ob *1.928*	V4−O31	1.9217(5)	1.927	0.77	0.77	13.66	9.59	0.03	−4.1	−3.98	21.72	−18.09
		V4−O32	1.9427(5)		0.74		12.76		0.03	−3.94	−3.82	20.52	−17.09
	VIII−Ob *2.006*	V1−O32	1.9981(6)	2.013	0.65	0.62	11.04	8.60	0.03	−3.25	−3.14	17.43	−12.77
		V1−O31	2.0205(5)		0.58		10.04		0.03	−2.60	−2.52	15.16	−8.37
		V2−O31	2.0040(5)		0.65		10.95		0.03	−3.25	−3.17	17.36	−12.70
		V2−O32	2.0268(6)		0.58		10.02		0.13	−2.76	−2.43	15.21	−8.77
V−Oc	VII−Oc *1.880*	V3−O20	1.8504(6)	1.883	0.79	0.84	14.49	10.63	0.03	−4.1	−3.96	22.55	−18.83
		V3−O25	1.8716(5)		0.85		14.99		0.06	−4.91	−4.64	24.54	−24.63
		V5−O23	1.8795(5)		0.86		14.83		0.04	−4.91	−4.72	24.46	−26.38
		V5−O24	1.8911(5)		0.86		14.61		0.07	−5.1	−4.72	24.47	−26.97
	VIII−Oc *1.821*	V1−O23	1.8132(6)	1.826	1.06	0.97	17.77	12.41	0.05	−6.88	−6.54	31.19	−44.12
		V1−O20	1.8338(6)		0.97		17.45		0.04	−5.83	−5.59	28.87	−32.89
		V2−O24	1.8141(6)		1.05		17.55		0.02	−6.55	−6.45	30.54	−42.70
		V2−O25	1.8240(6)		1.00		17.70		0.04	−6.07	−5.82	29.54	−36.40
V−Od	VII−Od *1.832*	V3−O22	1.8871(6)	1.831	0.94	0.95	16.00	12.19	0.11	−5.76	−5.2	26.96	−32.90
		V5−O22	1.8795(6)		1.03		16.58		0.09	−6.65	−6.12	29.35	−42.65
V−Oe	VI−Oe *1.688*	V4−O27	1.6848(5)	1.697	1.42	1.35	24.62	17.42	0.04	−9.55	−9.21	43.39	−80.50
		V4−O21	1.7059(6)		1.29		24.66		0.04	−8.30	−7.98	40.94	−60.71
	VII−Oe *2.049*	V3−O21	2.0183(6)	2.032	0.57	0.55	9.88	8.46	0.08	−2.64	−2.43	14.95	−7.80
		V5−O27	2.0697(6)		0.54		8.78		0.05	−2.49	−2.38	13.75	−7.45
V−Of	VIII−Of *1.609*	V1−O13	1.6189(6)	1.614	1.79	1.66	29.10	22.48	0.04	−13.67	−13.18	55.96	−133.72
		V2−O12	1.6230(6)		1.61		28.85		0.09	−11.74	−10.76	51.36	−102.93
V−Og	VII−Og *1.603*	V3−O11	1.6115(6)	1.605	1.71	1.68	30.96	22.32	0.06	−12.28	−11.54	54.78	−114.57
		V5−O10	1.6120(6)		1.75		30.17		0.11	−13.54	−12.24	55.95	−124.92

[b] Different V−O distances (Å) are reported according to the vanadium and oxygen classification. This work (estimated standard deviations in parentheses), theoretical data from Kempf [47] and average values from 37 structures retrieved in CSD bases (second column in italic). Results of the topological analysis of charge density at (3,-1) BCP of the DV anion. Our results ($\rho(r_{cp})$ is the electron density at the BCP (e Å^{-3}), $\nabla^2\rho(r_{cp})$ is Laplacian at the BCP (e Å^{-5}), ε is ellipticity, λ_1, λ_2, λ_3 are the eigenvalues at the BCP, H is the total energy density (kcal mol^{-1}) are compared to the $\rho(r_{cp})$ and $\nabla^2\rho(r_{cp})$ theoretical data.[47]

is protonated, and hydrogen atom H2b is bonded to N3b leading to a charge of +1e for the molecule. The cytosinium A is protonated, a half of hydrogen atom H2a is bonded to N3a, with a charge of +0.5e. This hydrogen lies on the crystallographic center of symmetry. The asymmetric unit also contains two sodium atoms. Both sodium atoms (Na1 and Na2) are in octahedral coordination.

The crystal structure of the title compound is stabilized by an extensive network of hydrogen bonds which involve the DV anions, the cytosine and the water molecules. Table 3 reports the most significant hydrogen bond features according to the usual criterion (d(D···A) < 3.5 Å). Symmetry codes used in the text are defined in caption 4. The structure contains several varieties of intermolecular interactions such as O−H···O, N−H···O, N−H···N, C−H···O, and O−H···N. There is a strong hydrogen bonding interactions between bridging oxygen atoms O2x of the DV anion and the N4 atoms of the cytosine. The DV anions are connected via oxygen−sodium−oxygen chains in the (001) plane. In an other direction, the anions are connected via hydrogen bonds (medium and weak) with cytosine B and cytosine C.

Description of Covalent Bonds in DV Anion. Static deformation density maps for horizontal and vertical *XY*, *XZ* and *YZ* planes are represented in Figure 3. As expected, there is a significant charge accumulation on the shorter V−O bond. For the longest bond we do not observe any deformation density. The deformation density maps display regions of electron density accumulation around all vanadium atoms. These accumulations are oriented toward the Oa atoms. Since the V−Oa distance is the longest V−O bond in the cage (yellow color in Figure 3), the density accumulations can be interpreted as the counterpart of the charge depletion occurring along the opposite and shorter V−O bonds (red color). Differences in static electron density maps in the vicinity of oxygen atoms are well expressed. Around the O22 oxygen atom (Figure 3a) we see, symmetrically distributed, an electron density accumulation in the direction of the bonds while in the vicinity of the O21 and O27 atoms, the electron density is asymmetrically shared. This is an expected result because all the vanadium atoms are not in the same environment. The O22 atom is connected to two V atoms (V3 and V5) which are in the same environment, having a V−O distance of 1.8871(6) Å and 1.8795(6) Å, respectively. Therefore, we can observe a symmetrical density accumulation around O22 (Figure 3a). As it is shown in Figure 3a, O27 and O21 atoms are located between two different types of V atoms; in this case, the charge accumulation is in the direction of the shortest bond O27−V4. The highest electron density peaks (Figure 3b) are found between V1−O13 followed by those in V2−O12 because the distance V1−O13 (1.6189(6) Å) is shorter than the V2−O12 distance

Table 3. Distances (Å) and Angles (deg) of the Hydrogen Bonds (D, Donor; A, Acceptor)[c]

	D−H···A	*d*(H−A)	*d*(D··A)	∠DHA	d_1	d_2	$\rho(r_{cp})$	$\nabla^2\rho(r_{cp})$	ε	λ_1	λ_2	λ_3	$H(r_{cp})$
O−H···O	O1w−H1w′···O32	1.6924(5)	2.6535(8)	174.49(5)	1.692	0.533	0.20	6.39	0.04	−0.95	−0.91	8.25	8.78
	O2w−H2w′···O20$^{(v)}$	1.7049(6)	2.672(1)	176.92(6)	1.705	0.547	0.18	5.96	0.02	−0.83	−0.82	7.60	8.72
	O4w−H4w′···O31$^{(x)}$	1.7583(5)	2.7201(9)	177.40(5)	1.758	0.570	0.15	5.30	0.02	−0.62	−0.61	6.53	8.28
	O2w−H2w ···O21	1.8311(5)	2.753(1)	159.29(6)	1.831	0.668	0.14	3.49	0.30	−0.75	−0.57	4.82	4.62
	O5w−H5w′···O2b	1.8439(7)	2.777(1)	162.16(5)	1.844	0.662	0.11	3.51	0.31	−0.66	−0.5	4.67	5.54
	O3w−H3w′···O12$^{(x)}$	1.8620(6)	2.8132(9)	169.01(5)	1.862	0.654	0.10	3.58	0.29	−0.53	−0.42	4.53	6.03
	O5w−H5w···O25$^{(vii)}$	1.8921(6)	2.8356(9)	164.95(5)	1.892	0.647	0.09	3.62	0.22	−0.37	−0.30	4.29	6.46
	O3w−H3w···O2c$^{(ix)}$	1.9730(9)	2.841(1)	148.40(6)	1.973	0.769	0.10	2.31	0.33	−0.53	−0.4	3.23	3.39
	O2w−H2w′···O11$^{(iv)}$	2.8023(7)	3.306(1)	113.23(5)									
	O4w−H4w···O11$^{(vii)}$	2.8271(7)	3.315(1)	112.60(5)									
	O1w−H1w′···O12	2.9091(7)	3.449(1)	115.72(5)									
	O2w−H2w···O11$^{(iv)}$	2.9382(7)	3.306(1)	103.95(5)									
	O5w−H5w···O12$^{(vii)}$	2.9378(7)	3.302(1)	103.67(5)									
	O3w−H3w′···O13$^{(x)}$	2.9904(6)	3.3954(9)	106.75(4)									
N−H···O	N1a−H1a··O4w	1.7006(7)	2.705(1)	173.70(6)	1.701	0.531	0.19	6.26	0.04	−0.96	−0.92	8.14	9.03
	N4c−H3c···O2b$^{(ii)}$	1.7475(8)	2.756(1)	173.49(6)	1.748	0.595	0.27	3.74	0.02	−1.56	−1.53	6.84	−0.35
	N1b−H1b···O1w	1.7519(7)	2.757(1)	173.48(6)	1.752	0.597	0.17	4.32	0.26	−0.99	−0.79	6.1	5.52
	N4a−H3a···O2a$^{(i)}$	1.8324(7)	2.841(1)	177.12(6)	1.834	0.641	0.20	3.01	0.03	−1.11	−1.08	5.21	1.40
	N4b−H4b···O24$^{(viii)}$	1.8536(5)	2.8603(9)	174.92(5)	1.854	0.632	0.09	3.77	0.52	−0.46	−0.3	4.53	6.78
	N4b−H3b···O2c$^{(ii)}$	1.866(1)	2.874(2)	178.47(7)	1.866	0.619	0.09	3.86	0.38	−0.42	−0.31	4.59	7.06
	N4a − H4a···O23$^{(i)}$	1.8678(6)	2.8581(9)	166.44(6)	1.867	0.707	0.12	2.80	0.66	−0.77	−0.47	4.04	3.86
	N4c−H4c···O22$^{(iii)}$	1.8798(5)	2.875(1)	169.84(1)	1.879	0.695	0.13	2.53	0.49	−0.66	−0.45	3.64	3.06
	N1c−H1c···O2w	2.288(1)	3.084(2)	155.6(1)									
	N1c−H1c···O20$^{(v)}$	2.4963(5)	3.1466(6)	135.8(1)									
	N4c−H4c···O25$^{(viii)}$	2.7832(6)	3.373(1)	117.91(6)									
	N4c−H4c···O24$^{(viii)}$	2.9210(6)	3.407(1)	110.55(6)									
N−H···N	N3b−H2b···N3c$^{(ii)}$	1.8087(9)	2.816(1)	173.39(5)	1.801	0.594	0.39	1.78	0.03	−2.3	−2.22	6.31	−11.72
	N3a−H2a···N3a$^{(i)}$	1.8491(8)	2.838(2)	167.72(2)									
C−H···O	C5b−H5b···O10$^{(vi)}$	2.0702(6)	3.150(1)	98.22(6)									
	C5a−H5a···O10$^{(i)}$	2.2430(7)	3.304(1)	165.93(6)	2.242	0.865	0.04	1.25	0.60	−0.16	−0.1	1.52	2.28
	C6c−H6c···O11$^{(iv)}$	2.4177(8)	3.222(2)	144.9(1)	2.417	1.016	0.08	0.95	0.08	−0.24	−0.22	1.42	0.84
	C6b−H6b···O10	2.6784(7)	3.292(1)	115.46(6)									
	C5c−H5c···O22$^{(iii)}$	2.6819(5)	3.489(1)	130.78(6)									
	C6b−H6b···O23	2.7570(6)	3.147(1)	100.89(6)	2.758	1.281	0.06	0.70	0.29	−0.16	−0.13	0.99	0.75
	C6a−H6a···O11$^{(vii)}$	2.8154(7)	3.384(1)	112.86(6)									
	C6c−H6c···O22$^{(iv)}$	2.8392(5)	3.390(1)	119.2(1)									

[c] Estimated standard deviations are given in parentheses. (i) = $-x,-y+1,-z+2$; (ii) = $-x+1,-y+1,-z+2$; (iii) = $x,+y,+z+1$; (iv) = $-x+2,-y,-z+1$; (v) = $x+1,+y,+z$; (vi) = $-x+1,-y,-z+2$; (vii) = $-x+1,-y+1,-z+1$; (viii) = $+x,+y,+z-1$; (ix) = $x-1,+y,+z$; (x) = $-x,-y+1,-z+1$. Results of the topology analysis are given. Units are given in Table 2. d_1 and d_2 are BCP−atoms distance (Å).

Table 4. Experimental Determination of the d Orbital (e) Populations of the Vanadium in the DV Anion

	V(I)	V(II)	V(III)
d_{z^2}	0.57(4)	0.70(5)	0.68(5)
$d_{x^2-y^2}$	0.68(4)	0.61(5)	0.68(5)
d_{xy}	0.60(8)	0.60(9)	0.61(8)
d_{xz}	0.62(4)	0.66(5)	0.57(5)
d_{yz}	0.56(4)	0.64(5)	0.67(5)
d orbital population	3.03(5)	3.20(5)	3.20(5)

(1.6230(6) Å). We have found for O61 atom (Figure 3a) a practically spherical electron distribution, which is in a good agreement with the theoretical calculation results.[46,47] The main differences could be attributed to the hydrogen bonding network. The deformation density is symmetrically distributed in the direction of the bonds because of very similar distances (O31−V2 = 2.0040(5) Å and O31−V1 = 2.0205(5) Å; O32−V1 = 1.9981(6) Å and O32−V2 = 2.0268(6) Å). Additionally, the lone pairs of the monocoordinated oxygen atoms (O1x) are clearly visible.

Topological parameters of the electron density for the (3,-1) BCP′s of DV containing bonds are given in Table 2. All V−O bonds are characterized by a very large positive curvature at the BCP along the direction of the bond path (λ_3). It has been established that the positive values of $\nabla^2\rho(r_{cp})$ are characteristic of "closed-shell" interactions governed by the contraction of the charge density toward each of interacting nuclei.[84] According to topological features, the difference between the V−O bonds is more pronounced. The $\rho(r_{cp})$ values for the shortest V−O bond are compared to those of the longest V−O bond. Correlation between experimental and theoretical data is very good, except $\rho(r_c)$ value for VII−Od. This is not surprising because the VII−Od[47] distance is 1.831 Å compared to our experimental result of 1.8871(6) Å. We observe that $\rho(r_{cp})$ at the BCP is a decreasing function of the interatomic distances. The topological results fit quite well with the classification of the oxygen types and the vanadium types in the DV anion. The dispersion of the data is very small, leading to a quantitative agreement. Aditionnaly, $d_1 + d_2$ is always very close to the interatomic distance, except for three bonds V3−O20, V3−O22, and V5−O22; the position of the BCP is generally at the middle of the bond, except for the shortest V−O distance where larger discrepancies are observed. The total energy density $H(r_{cp})$ according to the Abramov formula[59] has also been calculated and presents a quite good behavior leading to significant energy for short V−O bonds. The analysis of the total density through the existence of the BCP and the

(84) Bader, R. F.; Preston, H. J. T. *Int. J. Quantum Chem.* **1969**, *3*, 327.

Table 5. Experimental and Theoretical Net Atomic Charges (e) for Vanadium Atoms in a DV Anion

		experimental				theoretical	
		$Na_3[V_{10}O_{28}](C_4N_3OH_5)_3(C_4N_3OH_6)_3\cdot 10H_2O$, this work			$(NH_4)_6V_{10}O_{28}\cdot 6H_2O$, Bogdanovic et al.[52]	$[V_{10}O_{28}]^{6-}$, Henry[49]	$[V_{10}O_{28}]^{6-}$, Kempf et al.[47]
atom	type	multipole refinement	AIM	κ refinement	κ refinement	PACHA	Mulliken
V4	I	+1.97(5)	+1.688	+1.94(5)	+2.0(1)	+1.514	+2.13
		+1.97(5)	+1.688	+1.94(5)	+1.9(1)	+1.514	+2.13
V3	II	+1.79(5)	+1.540	+1.85(5)	+1.7(1)	+1.865	+2.04
		+1.79(5)	+1.540	+1.85(5)	+1.8(1)	+1.865	+2.04
V5	II	+1.81(5)	+1.509	+1.71(5)	+1.6(1)	+1.870	+2.04
		+1.81(5)	+1.509	+1.71(5)	+1.6(1)	+1.870	+2.04
V1	III	+1.80(5)	+1.533	+1.74(5)	+1.6(1)	+1.780	+2.05
		+1.80(5)	+1.533	+1.74(5)	+1.6(1)	+1.780	+2.05
V2	III	+1.80(5)	+1.535	+1.78(5)	+1.7(1)	+1.766	+2.05
		+1.80(5)	+1.535	+1.78(5)	+1.6(1)	+1.766	+2.05

Table 6. Experimental and Theoretical Net Atomic Charges (e) and EP (e $Å^{-1}$) at the Molecular Surface in the Vicinity of the Oxygen Atoms of the DV Anion

		experimental						theoretical			
		$Na_3[V_{10}O_{28}](C_4N_3OH_5)_3(C_4N_3OH_6)_3\cdot 10H_2O$, this work				$(NH_4)_6V_{10}O_{28}\cdot 6H_2O$, Bogdanovic et al.[52]		$[V_{10}O_{28}]^{6-}$, Henry[49]		$[V_{10}O_{28}]^{6-}$, Kempf et al.[47]	
		multipole refinement	κ refinement		AIM	κ refinement		PACHA		Mulliken	ab initio SCF
		EP	charge	EP	charge	EP	charge	EP	charge	EP	charge	EP
O61	a		−0.88(5)		−0.724		−0.7(1)		−0.861		−1.27	
O31	b	−8.7	−0.97(5)	−8.2	−0.873	−8.7	−0.9(1)	−8.5	−0.726	−7.4	−1.04	−8.2
O32			−1.08(5)		−0.918		−0.6(1)		−0.713			
O24	c	−7.2	−0.90(5)	−6.9	−0.857	−7.1	−1.2(1)	−7.1	−0.666	−6.1	−0.93	−6.8
O25			−0.84(5)		−0.799		−0.6(1)					
O20			−0.81(5)		−0.808		−1.0(1)					
O23			−0.91(5)		−0.900		−0.7(1)					
O22	d	−6.9	−0.93(5)	−6.6	−0.797	−6.8	−1.0(1)	−6.9	−0.686	−5.8	−0.94	−6.5
O21	e	−7.4	−0.87(5)	−7.1	−0.783	−7.4	−0.8(1)	−7.2	−0.635	−6.4	−0.82	−7.0
O27			−0.92(5)		−0.733		−0.5(1)					
O13	f	−6.2	−0.63(5)	−5.9	−0.573	−6.2	−1.1(1)	−6.4	−0.555	−5.3	−0.63	−5.9
O12			−0.81(5)		−0.668		−0.7(1)					
O11	g	−5.8	−0.84(5)	−5.6	−0.717	−5.8	−0.5(1)	−5.7	−0.560	−4.9	−0.66	−5.5
O10			−0.65(5)		−0.620		−1.2(1)					

analysis of the deformation density lead to similar results and give the first experimental description of V−O bonds in a POV entity.

Description of Hydrogen Bonds. Topological analysis of the charge density is also a very useful tool for the characterization of hydrogen bonds.[85] It is interesting to compare accurately the results of the topology and the determination of the existence of hydrogen bonds using simple geometrical parameters (d(D···A) < 3.5 Å) (Table 3). The number of significant hydrogen bonds decreases from 37 to 20. As expected, all hydrogen-BCPs are of (3,-1) type. Hydrogen bonds are considered as closed-shell interaction because they display $\nabla^2\rho(r_{cp}) > 0$ and small $\rho(r_{cp})$ values. The O−H···O and N−H···O interactions are found to be the strongest and present higher $\rho(r_{cp})$ value than N−H···N and C−H···O ones. The $\rho(r_{cp})$ values for all types of bonds are in the range of $\rho(r_{cp})$ magnitudes previously reported for this kind of bonds.[86] For $\rho(r_{cp})$ and $\nabla^2\rho(r_{cp})$ we observed an exponential function of the interatomic distances. We have observed an exponential behavior of the eigenvalue λ_3 versus d(H···O) in all D−H···O interactions. The correlation between the positive curvature λ_3 and the interatomic distance for our result is especially excellent ($y = 387.2e^{-2.34x}$, $R^2 = 0.933$) and in a quantitative agreement with the results obtained previously[85] ($y = 245.7e^{-2.11x}$, $R^2 = 0.925$).

Observation of the static deformation maps indicates that the accumulation (number of contours at the point intersecting the bond) of the lone pair directed toward the hydrogen of the water molecule is clearly a function of the interatomic distance d(H···A) (Figure 4a). The height of the Ow−Hw deformation density peaks remains in the range of 0.5 to 0.6 e $Å^{-3}$, while for a same d(Hw···O) the peak height of the static deformation density involved in the interaction could vary within three contours. Nevertheless, the shortest O···H distance ($d_{H1w'\cdots O32}$ = 1.6924(5)Å) exhibits the highest density peak. The lone pair electron density peak height (maximum contour level of the lone pair) is 0.5 e $Å^{-3}$ that is in relative agreement with the highest $\rho(r_{cp})$ and $\nabla^2\rho(r_{cp})$ values observed at the BCP. The observation of the electron deformation density maps containing N−H···O hydrogen bond types reveals the following: (i) the intensity of the lone pair is less pronounced than in the O−H···O bond for a similar A···H distance, (ii) the H−N deformation bond exhibits a more delocalized deformation density cloud than the

(85) Espinosa, E.; Molins, E.; Lecomte, C. *Chem. Phys. Lett.* **1998**, *285*, 170.

(86) Espinosa, E.; Souhassou, M.; Lachekar, H.; Lecomte, C. *Acta Crystallogr.* **1999**, *B55*, 563.

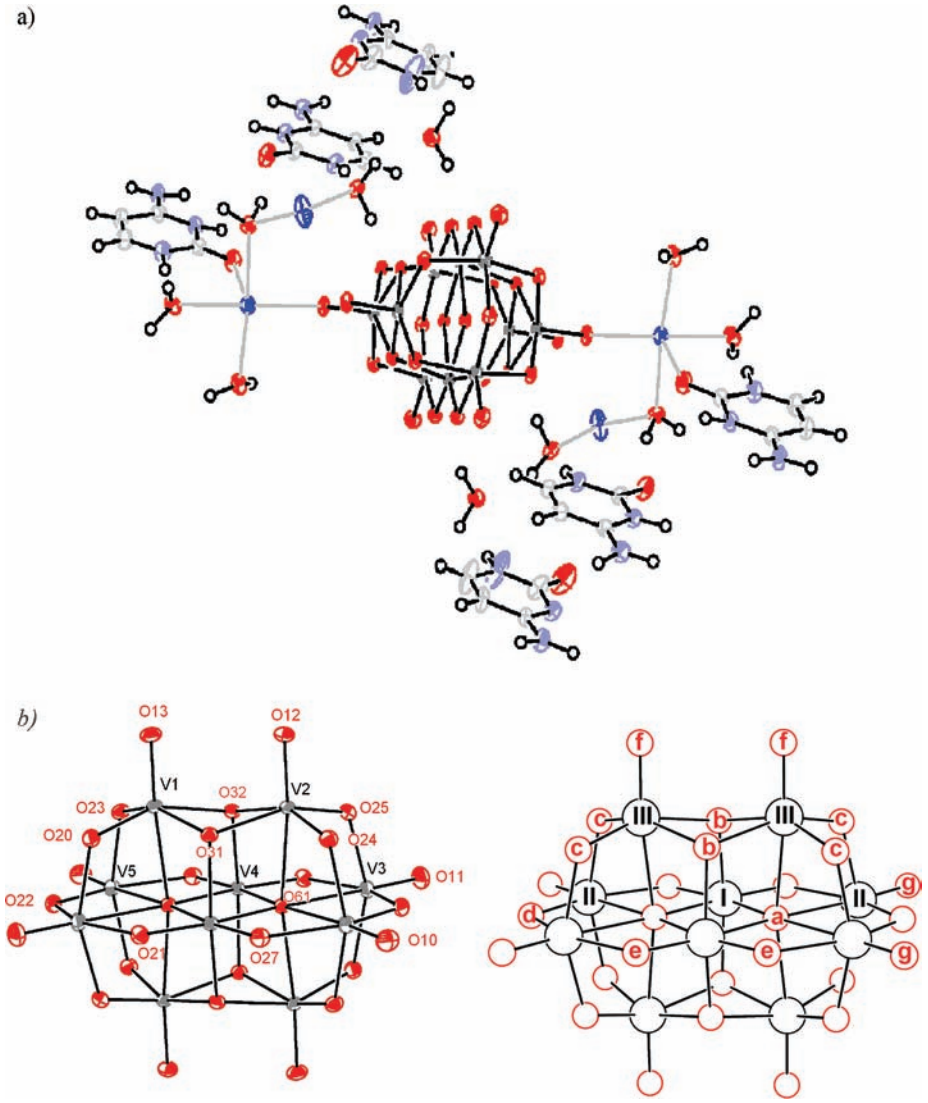

Figure 1. (a) ORTEP view of the Na_3 $[V_{10}O_{28}]$ $(C_4N_3OH_5)_3(C_4N_3OH_6)_3 \cdot 10H_2O$ structure and, (b) labeling scheme and type of atoms for the DV anion.

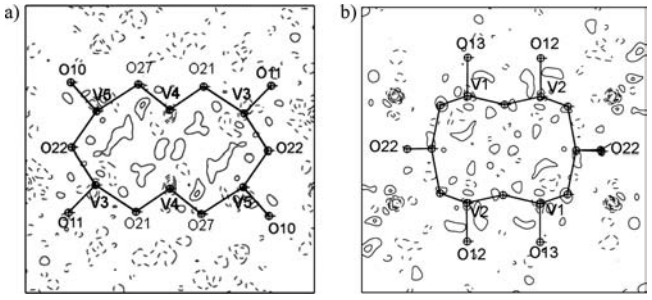

Figure 2. Residual electron density maps. (a) DV-horizontal plane (plane containing O10, O11, O21, O27, O22, O61, V3, V4, and V5 atoms), (b) DV-vertical-*XZ* plane (plane containing O12, O13, O22, O61, V1, and V2 atoms); O61 oxygen atoms are omitted. Contour intervals are 0.1 e $Å^{-3}$. Negative contours are dashed.

corresponding one in the Ow−Hw bond (Figure 4b). Oxygen atom O24 is involved in one strong bond, $O24^{(viii)}$, H4b and N4b, but the oxygen lone pair is shifted toward N−H···O hydrogen bonds. O22 presents an interesting behavior; the strongest hydrogen bond is N4c−H4c···O22 $^{(iii)}$, with $d_{H\ldots A}$ = 1.8798(5) Å, but the oxygen lone pair is clearly in the direction of the H5c hydrogen. That feature means that the N−H···O interaction is not strong enough to induce a shift of the oxygen lone pair. On the opposite, the O−H···O contacts exhibit strong interaction. We can conclude that the O−H···O interaction is stronger than the N−H···O one. Moreover, the lone pair exhibits higher contours measured at the maximum of the lone pair (0.5; 0.3; 0.4 e.A^{-3} for the O−H···O bond) and (0.2; 0.3; 0.3 e $Å^{-3}$ for the N−H···O bond). The C−H···O bond belongs to the category of weak or very weak hydrogen bonds.[87] For only three C−H···O hydrogen bonds, we have found a BCP. The $\rho(r_{cp})$ and $\nabla^2\rho(r_{cp})$ values for these bonds are very small and characteristic of weak hydrogen bonding.[88] It has been already noticed that it is difficult to observe electron density deformation for such a bond. This trend remains verified for the C−H···O bonds in our compound. That observation does not indicate that there is no interaction but that this interaction is not detectable using the tool of the static electron deformation density.

(87) Desiraju, G. R.; Steiner, T. In *The Weak Hydrogen Bond in Structural Chemistry and Biology*; Oxford Univ. Press: Oxford, 1999.
(88) Kubicki, M.; Borowiak, T.; Dutkiewicz, G.; Souhassou, M.; Jelsch, C.; Lecomte, C. *J. Phys. Chem.* **2002**, *B106*, 3706.

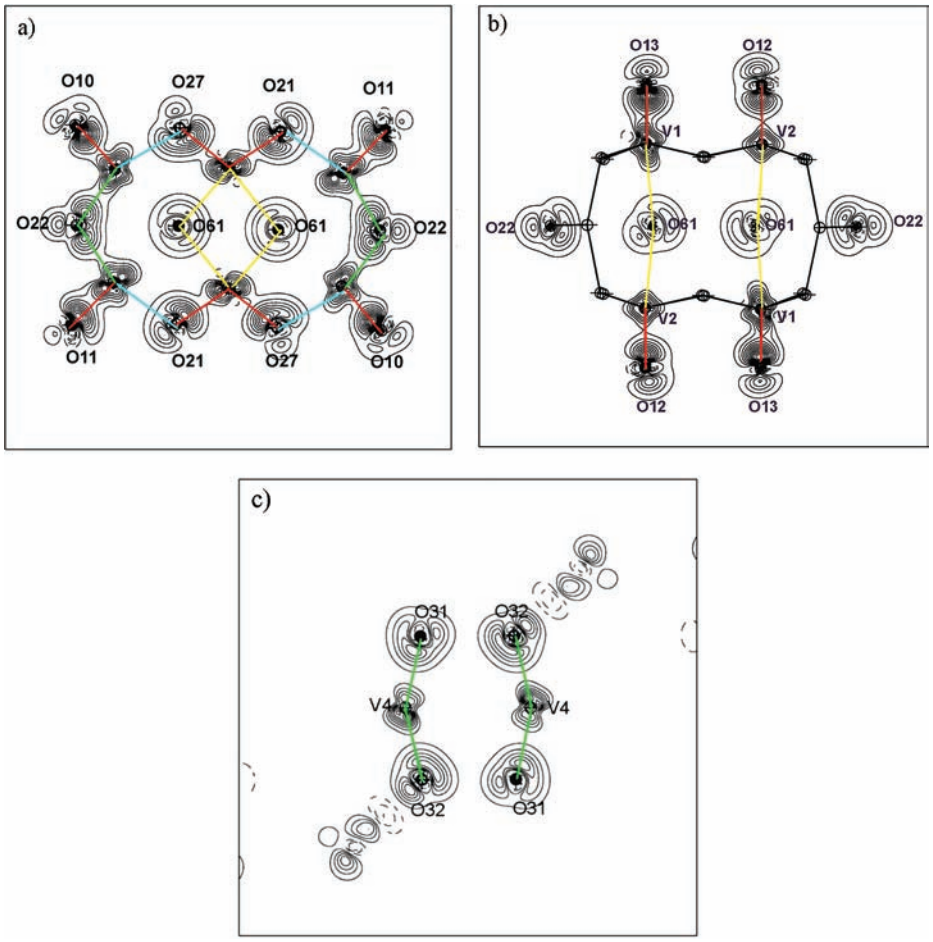

Figure 3. Static model deformation density. Planes (a) and (b) and contours as defined in Figure 2. (c) DV-vertical-YZ (plane containing O31 O32 and V4 atoms). The longest V−O bonds (VI−Oa, VII−Oa, VIII−Oa) in the cage are in yellow, the medium bonds are in green (VII−Od) and blue (VII−Oe) color and shortest V−O bonds (VI−Oe, VIII−Of, VII−Og) are in red color. The other bonds are in dark color.

d-Orbital Populations of the Vanadium Atoms. Holladay et al.[62] have demonstrated that a linear combination of the multipole parameters lead to an experimental determination of the d-orbital populations.[53] These results can give at least a quantitative agreement between experiment and theory. This was, for example, the case of a chromium complex[89,90] or other metal transition complexes.[62,91] To our knowledge, no such experimental 3d-orbital populations have been published concerning a vanadate compound. Metal coordination are slightly distorded octahedra, therefore we have chosen to refine the vanadium in the symmetry 1 leading to P_{lm} parameters ($l = 0$, 2, 4) according to Holladay et al.[62] For all V atoms, the z axis is chosen in the direction of the closest atom, and the x axis toward the second closest atom. We have determined for each vanadium atom the d-orbital populations (Table 4). Total d-orbital population analysis is coherent with an oxidation state for the V atoms of +2 in the $4s^0d^x$ configuration (x varying from 3.03 for VI to 3.20 for VII and VIII). The results are in good agreement with the features observed in the crystal structure, deformation density maps, and topological analysis. Since a high charge concentration and higher ρ value is found on the shorter V−O bond, the highest population value is found in the d_{z^2} orbital for VII and VIII atoms. The highest population for $d_{x^2-y^2}$ orbital is found for V1 and V2. For V4, $d_{x^2-y^2}$ in the plane O21−V4−O31 and d_{xz} which is along the bond V4−O21 exhibit the highest population values.

Atomic Net Charges. We have calculated the atomic net charges to get insight into the reactivity of oxygen atoms. A κ-refinement has been carried out without charge transfer between cytosine molecules and DV anion; therefore only separate and comparative discussions on each entity make sense. A set of final refinement cycles has been performed without restraints on charge tranfer leading to very similar results. That indicates that there is no significant charge transfer between DV and the organic moiety as well as the water molecules or the Na^+ ion. Therefore, we will only discuss the results without charge transfer to be easily comparable to the experimental results or theoretical calculations performed on $[V_{10}O_{28}]^{6-}$ anion. The κ coefficients, experimental atomic net charges (derived from different methods[51] on the two compounds $(NH_4)_6$ $[V_{10}O_{28}]\cdot 6H_2O$ and $Na_3[V_{10}O_{28}](C_4N_3OH_5)_3$ $(C_4N_3OH_6)_3$ $\cdot 10H_2O$), and data from

(89) Spasojević-de Biré, A.; Nguyen, Q. D.; Becker, P. J.; Benard, M.; Strich, A.; Thieffry, C.; Hansen, N. K.; Lecomte, C. In *Application of charge density research to chemistry and drug design*; NATO ASI Series; Jeffre, G. A., Ed.; Plenum Publisher: New York, 1991; p 385.
(90) Spasojević-de Biré, A.; Dao, N. Q.; Hansen, N. K.; Fisher, E. O. *Inorg. Chem.* **1993**, *32*, 5354.
(91) Lee, C. R.; Wang, C. C.; Chen, K. C.; Lee, G. H.; Wang, Y. *J. Phys. Chem.* **1999**, *A103*, 156.

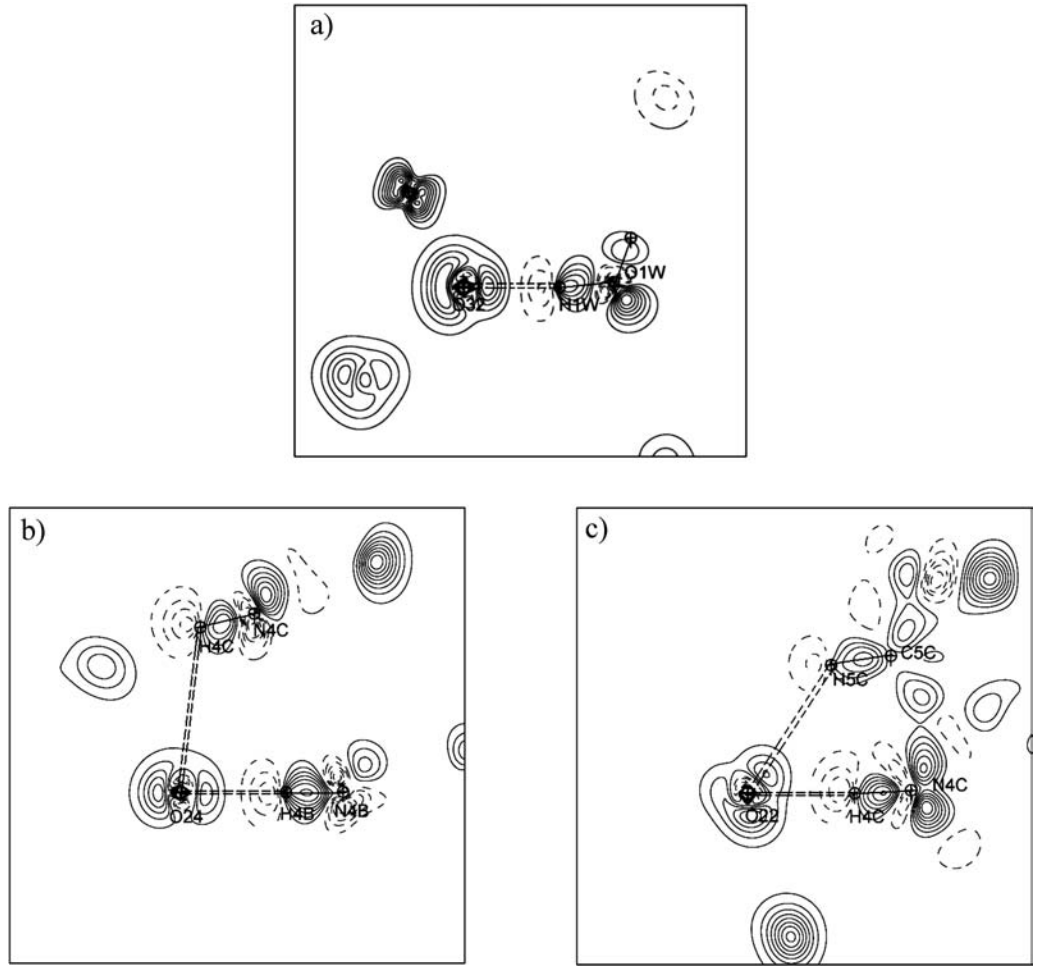

Figure 4. Static deformation density of D−H···A hydrogen bonds. Planes containing (a) O32, H1w′, and O1w, (b) O24, H4c$^{(viii)}$, and H4b$^{(viii)}$ and (c) O22, H4c$^{(viii)}$, and H5c $^{(viii)}$. Contours as defined in Figure 2.

theoretical calculations[47,49] of the DV anion are compiled in Tables 5 and 6. As expected, some differences are found between charges derived from the κ-refinement and from AIM analysis[56] of the experimental model density. According to the results of the κ-refinement, the vanadium atom carries an average positive charge of $+1.80$ e. In the polyanions, the internal V4 have the highest charges, whatever the method, which is in good agreement with the results from theoretical calculations.[47] The DV oxygen atom electron densities are slightly expanded ($\kappa \leq 1.0$). For the oxygen atoms, the AIM charges are less negative than the monopole charges derived from the κ-refinement. The negative charge on oxygen atoms consistently increases with the number of connected metal atoms. This trend is both observed in experimental and theoretical studies. Generally, net atomic charges derived from experimental and theoretical densities are in good agreement, despite the fact that the theoretical calculations are based on an isolated molecule. Nevertheless, the AIM analysis gives a more rigorous definition of the charges of the atoms in molecules, thus providing a more reliable framework for comparison between molecules and between experiment and theory.[91,92] Therefore, for oxygen atoms of type b and type c which are involved in the strongest hydrogen bond (acceptor atom), we have found the most negative value of atomic net charge.

Electrostatic Potential. To obtain information on the potent reactivity of the compound, it is useful to color with the EP values the reactive surface of the molecule; the most nucleophilic molecular regions correspond to the most negative EP. The experimental EP can be calculated at the final step of the three refinements (the κ-refinement, the multipole refinement, and using the AIM charges). The EP values at the three-dimensional isodensity surface (0.007 e Å^{-3}) of the DV anion are shown in Figure 5 (first column) using the maximum color scale for the EP values on the molecular surface; the blue region correspond to -4.9 e Å^{-1} and the red value to -8.7 e Å^{-1}. To have a complete picture of the electrostatic properties of the DV in the vicinity of the oxygen atoms, we have reported in Table 6 the experimental and the theoretical EP (Figure 5, column 5 and 6) projected on the molecular surface of the DV anion in different environments or using different models.

The EP on the surface is negative on the whole molecular surface of the DV, as it is expected for an anion. Some differences are found between the values from the κ-refinement, from the multipole refinement, and from AIM charges. The greatest differences between the two

(92) Volkov, A.; Gatti, C.; Abramov, Y.; Coppens, P. *Acta Crystallogr.* **2000**, *A56*, 252.

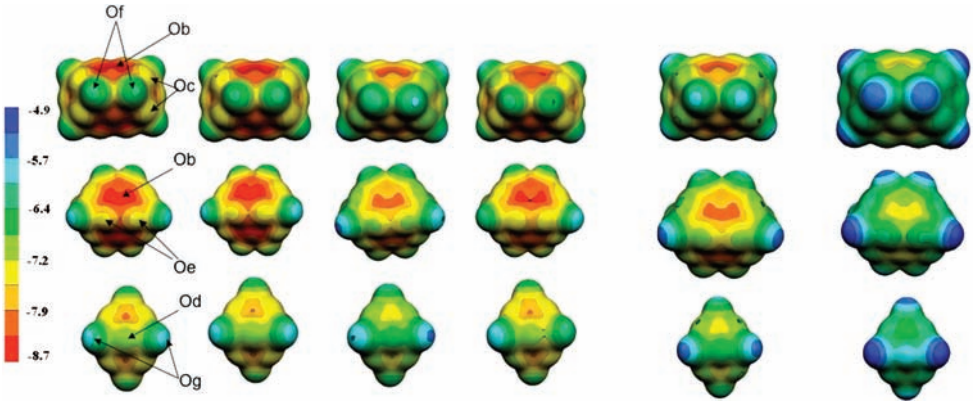

Figure 5. Experimental EP on the molecular surface (0.007 e Å^{-3}) (column 1−4). Column 1−3 $Na_3[V_{10}O_{28}](C_4N_3OH_5)_3(C_4N_3OH_6)_3\cdot 10H_2O$, column 4 $(NH_4)_6[V_{10}O_{28}]\cdot 6H_2O$. EP of the DV isolated from the crystal computed from the multipole refinement (column 1), from the charge determined by the AIM method (column 2), and by a κ refinement (columns 3 and 4). Theoretical EP (columns 5−6) computed from the charge determined by the Mulliken partitioning[47] (column 5) and by a PACHA partitioning[49] (column 6).

EP determinations are found in the vicinity of the Ob oxygen sites which are involved in strongest hydrogen bond. Because the multipole model is closer to reality than the κ one, the EP values obtained from the multipole refinement will be only discussed in the following paragraphs. The deepest minimum of the EP is found close to the Ob oxygen atoms, which are reported as the most negative atom in this structure. It means that these atoms are predominant locations for hydrogen-bond interactions. Similar results have been previously found from ab initio theoretical computations.[48−50] Therefore, we can confirm that the most basic accessible sites for protonation in the cage are oxygen atoms of type b. If we compare our experimental characterization of the EP at the molecular surface to those recalculated with the theoretical atomic charges (Mulliken[47] or PACHA charges[49]), one can observe that the Mulliken determination from an ab initio SCF calculation give very similar results to those obtained experimentally. This is clear in Figure 5, but also from the EP values reported in Table 6. On the contrary, the PACHA calculation seems not adequate to describe correctly the EP of the DV anion. Nevertheless, these calculations give the same trend (Ob possesses the most negative EP). There is a quantitative agreement between the same partitioning method used for different anions and an agreement between different partitioning method for the same anion. These very close values obtained on two different compounds clearly indicate that the properties obtained experimentally at a molecular level are transferable from an anion in a given environment to an anion in another environment.

Concluding Remarks and Further Applications

In this paper, we have characterized the chemical bonds, the net atomic charges and the electrostatic properties of $Na_3[V_{10}O_{28}](C_4N_3OH_5)_3(C_4N_3OH_6)_3\cdot 10H_2O$ derived from a high resolution X-ray diffraction experiment. One of the main results is that the EP found at the molecular surface could be considered as "transferable", that is, independent of its crystalline environment. This result strictly concerns the non-protonated DV anion. New ab initio calculations or experimental charge density studies have to be performed to determine the $[V_{10}O_{28}H_x]^{(6-)-x}$ ($x = 1$ to 5) EP. According to our results (rigidity of the $[V_{10}O_{28}]^{(6-)}$ anion, transferability of the EP values at the molecular surface of the anion), one can reasonably think that a same "transferability rule" would exist, the EP values at the molecular surface depending of the proton position on the oxygen of the $[V_{10}O_{28}H_x]^{(6-)-x}$.

As previously mentioned, the DV anion strongly inhibits proteins and enzymes. Since the DV anion is a rigid entity which remains the same in solution,[34] one can make some hypotheses to correlate the properties at the molecular level of the DV anion and its interaction with some biological targets. We will focus on the putative mechanisms of interaction/inhibition/activation and the possible better understanding of those mechanisms because of our very precise knowledge of the electronic and electrostatic properties of the DV anion. Therefore we will discuss the biological targets for which a crystallographic structure or electron microscopy features of the DV anion as a ligand is known, Ca^{2+}-ATPase[11−14] and Acid phosphatase A,[22] or with the biological targets for which a docking of DV has been performed.

A large family of ATP-dependent ion pumps, known as P-type ATPases, achieves active transport of cations. The determination of two Ca^{2+}-ATPase structures has been performed by X-ray crystallography[93,94] and cryoelectron microscopy.[15,95−97] The authors have demonstrated from biological inhibition of ATPase activity that two binding sites exist for the DV anion.[11,12,98] Unfortunately the low resolution of the structures concerned has not permitted such a precise determination. Therefore, only new docking modelization using our experimental EP and hydrogen bond predictions could give new information. Felts et al.[22] have reported the 1.75 Å resolution crystal structure of Acid phosphatase A complexed with the inhibitor orthovanadate, the first published structure for any member of this superfamily (2d1g code in the Protein Data Bank). In this structure, the DV anion is linked to the protein through three histidine and a lysine, asparagine, and to one water molecule (NH···O interactions with a N···O < 2.70 Å). It is

(93) Toyoshima, C.; Nakasako, M.; Nomura, H.; Ogawa, H. *Nature*. **2000**, *405*, 647.
(94) Toyoshima, C.; Nomura, H. *Nature* **2002**, *418*, 605.
(95) Stokes, D. L.; Green, N. M. *Biophys. J.* **2000**, *78*, 1765.
(96) Xu, C.; Rice, W. J.; He, W.; Stockes, D. L. *J. Mol. Biol.* **2002**, *316*, 201.
(97) Hinsen, K.; Reuter, N.; Navaza, J.; Stokes, D. L.; Lacapere, J. J. *Biophys. J.* **2005**, *88*, 818.
(98) Hua, S.; Inesi, G. *J. Biol. Chem.* **2000**, *275*, 30546.

interesting to note that the stronger hydrogen bond interactions between DV and the rest of the protein takes place on the most reactive oxygen atoms Ob, Oc, Oe. Therefore, these results show that the hydrogen bond behavior of the DV anion we have observed and described remains the same when the DV anion is bound to a protein.

Tiago et al.[21] have performed a docking study using the structure of truncated *Dictyostelium discoideum* myosin motor domain (S1dC code in the Protein Data Bank). These authors have used the theoretical results[47] for the modelization of the DV assuming that Ob and Oc oxygen atoms have a charge of −2 and the other oxygen atoms have a charge of −1, while the charge of the vanadium atom was fixed to +2.4. We have computed the EP at the molecular surface of the DV anion. The values vary from −6.5 e $Å^{-1}$ to −9.81 e $Å^{-1}$ compared to those determined experimentally or theoretically by Kempf et al.[47] (Table 6). The approximation chosen by Tiago et al.[21] gives significantly different EP values at the molecular surface, which could imply some uncertainties in the docking results. Pezza et al.[16] have studied the inhibition of the ATPase activity and the DNA binding capability of bacterial MutS. Docking of DV on the ATP-binding region of MutS showed that the energetically more favorable interaction of this compound would take place with the complex MutS-ADP-Mg, suggesting that the inhibitory effect could be produced by a steric impediment of the protein ATP/ADP exchange. New docking, using our precise determination of the electronic and electrostatic properties of the DV anion, could improve these results. Nilius et al.[99] have tested the effects of the DV on TRPM4 a Ca^{2+}-activated voltage dependent monovalent cation channels, whose activity is potently blocked by intracellular ATP^{4-}. The authors have identified that the site of DV action resides in the C-terminus of TRPM4. In this case, a docking study using our DV properties could also give new understanding of the mechanism.

To get a better understanding of the inhibition process of Ca^{2+}ATPase, Na^+/K^+ATPase we have investigated the influence of DV on Synaptic Plasma Membrane (SPM) Na^+/K^+ATPase and SPM Ca^{2+}-ATPase activities.[14] The results indicate that the enzyme activity at each DV concentration represents the sum of the activity of two Na^+/K^+-ATPase isoforms, differing in their affinity, that is, in their sensitivity toward DV. This two-step mechanism sounds pertinent according to the possibility of DV to bind with different type of interactions (strong or weak H-bonds).

Therefore one can conclude the following: (i) the potent different types of interaction (strong and weak DH···O bonds). (ii) Our hydrogen bond predictions fit well with the only reported high resolution (2d1g) structure. (iii) Our atomic net charges, hydrogen bond, and cation interaction predictions could be suitably used in the docking computations and would probably give better results than the commonly used charges.

Acknowledgment. N.B.-P., A.S.d.B., and U.M. thank the French Foreign Ministry for a COCOOP support on this project. N.B.-P. and U.M. thank the Ministry of Science and Technological Development of the Republic of Serbia (Project 142047). This paper is a part of a joint Ph.D. thesis between the University of Belgrade, Faculty of Physical Chemistry and the Ecole Centrale Paris. J.C.P. thanks FCT, FEDER, POCI 2010, and PPCDT/QUI/56959/2004.

Supporting Information Available: Tables of atomic coordinates, thermal displacement parameters, bond lengths and bond angles, crystal structure references, figures of local coordinates scheme, molecular structure, crystal packing, experimental, dynamic and static deformation maps of different planes. This material is available free of charge via the Internet at http://pubs.acs.org.

(99) Nilius, B.; Prenen, J.; Janssens, A.; Voets, T.; Droogmans, G. *J. Physiol.* **2004**, *560*, 753.